Journal of Alloys and Compounds 617 (2014) 235–239

Contents lists available at ScienceDirect

Journal of Alloys and Compounds

journal homepage: www.elsevier.com/locate/jalcom

Chemical synthesis and microstructure of nanocrystalline RB_6 (R = Ce, Eu)

Bao Lihong, B. Wurentuya, Wei Wei, Li Yingjie, O. Tegus *

Inner Mongolia Key Laboratory for Physics and Chemistry of Functional Materials, College of Physics and Electronic Information, Inner Mongolia Normal University, Hohhot 010022, China

ARTICLE INFO

Article history:
Received 21 May 2014
Received in revised form 29 June 2014
Accepted 30 June 2014
Available online 9 July 2014

Keywords:
Nanocrystalline
Rare-earth hexaborides
Solid-state reaction
Microstructure

ABSTRACT

Nanocrystalline RB_6 (R = Ce and Eu) have been successfully synthesized by a solid-state reaction of CeO_2 and Eu_2O_3 with $NaBH_4$ at a temperature range of 900–1200 °C. Phase composition, grain morphology, microstructure and valence states of RB_6 were investigated by using XRD, FESEM, HRTEM and XANES measurements. Results show that all the synthesized hexaborides are composed of single-phase nanoparticles with cubic morphology. The FFT patterns of HRTEM images reveal that the hexaborides have a high crystallinity with CaB_6-type cubic structure. The present preparation technique is as a novel and invaluable for the developments of highly crystallized RB_6 nanoparticles.

1. Introduction

Rare-earth hexaborides (RB_6) as a multifunctional novel material have attracted many interests owing to their special electronic and magnetic performance. Among the rare-earth hexaborides, LaB_6 and CeB_6 as an excellent thermionic electron emitter were characterized by high brightness, thermal stability, low volatility and high mechanical strength [1–4]. SmB_6 as a topological Kondo insulator also has attracted much attention due to the manifestation of strong electronic correlations which give rise to exotic ground state [5–8]. NdB_6 [9] and EuB_6 [10] are extensively studied due to their complicated magnetic transport properties. In resistivity and specific-heat measurements, there are two magnetic phase-transition temperatures observed for EuB_6 at $T_c \approx 15.5$ and 12.6 K. GdB_6 [11] was reported to have the lowest work function. However, because of its relatively poor stability at high working temperature [12], it is more suitable for field emission electron source with high brightness at room temperature rather than thermionic cathode. Based on the above mentioned facts, there are great research prospects for rare-earth hexaborides, especially regarding to their excellent thermoemission, magnetic and topological insulator properties.

Recently, rare-earth hexaborides with nanostructure such as nanowires [13–16] and nanopowders [17–20] have attracted great interests in both scientific and technological areas. Since the nanowires have a very sharp tip with diameters of less than hundred nanometers, it is very well fit the purpose of higher brightness and lower energy spread for field emission transmission and scanning electron microscope. By comparison with nanowires, the RB_6 nanopowders have shown many superior properties. The various RB_6 nanopowders showed different absorption capabilities in near infrared rays (NIR) due to the different free electron plasmon energies such as 1.97 eV for LaB_6, 1.96 eV for CeB_6, 1.89 eV for PrB_6 and 1.90 eV for NdB_6, respectively [21]. Takeda et al. have reported that the LaB_6 nanopowder shows a largest NIR absorption among the RB_6 nanopowders [22]. Yuan et al. studied the particle size effects on the optical properties of the composites of LaB_6 nanopowder mixing with polymethyl methacrylate (PMMA) [23]. The result shows that when the particle size is about 70 nm, it has the best optical property among the composites. Above mentioned excellent optical property of RB_6 nanopowder will very well meet the unique approach to reduce solar heat, which also provide a potentially low-cost and high-productivity solution. More recently, Lai et al. have successfully prepared a core–shell structured LaB_6@C-SiO_2, which shows excellent NIR photothermal conversion property and bright blue emission under UV irradiation, and green emission under visible irradiation [24]. Therefore, the RB_6 nanopowder will be widely used for the commercial applications as transparent solar control substances such as PET films and PVB interlayers for automotive and architectural windows. Another important development in the RB_6 nanopowder is that a great improvement on the density, hardness and fracture toughness of the WC-10 Co alloys has been achieved by adding a small amount of LaB_6 nanopowder [25].

* Corresponding author.
E-mail address: tegusph@imnu.edu.cn (O. Tegus).

http://dx.doi.org/10.1016/j.jallcom.2014.06.207
0925-8388/

Up to now, many synthesis methods [26–30] have been developed to prepare the RB_6 nanopowder for a low reaction temperature, easy to handle precursors, simple process controlled and low cost. Here, we report a simple and novel method for preparing the nanocrystalline RB_6 (R = Ce, Eu) by a solid-state reaction of R_2O_3 with $NaBH_4$ in a continuous evacuating conditions. In this way, we have found the trivalent CeB_6 can be obtained using the mixed valence of CeO_2 as raw materials, which is confirmed by the study of X-ray absorption near edge structure (XANES). The effects of reaction temperature on the crystal phase, size and morphology were characterized by using XRD, FESEM and HRTEM.

2. Experiments

The CeO_2 (99.99% purity), Eu_2O_3 (99.9% purity) and $NaBH_4$ 99.0 purity) powder in a fixed molar ratios were mixed in an agate mortar for an hour. Then the mixtures were put into a quartz tube and placed in the resistance furnace at a reaction temperature in the range from 900 to 1200 °C for 2 h. Whole reaction was kept under a vacuum of 2×10^{-2} bar. The phase identification was examined by X-ray diffraction (Cu Kα radiation, Philips PW1830). The crystal morphology was characterized by field emission scanning electron microscope (FESEM: Hitachi SU-8010) and the microstructure is characterized by transmission electron microscopy (TEM: FEI-Tecnai F20 S-Twin 200 kV). The XANES measurement was carried out using synchrotron radiation at the BL-12A station of Photon Factory, Japan.

3. Results and discussion

3.1. Characterization of the raw materials

It is necessary to study the microstructure of raw materials because the particle sizes of raw materials have influence on the grain size of final products in solid-state reaction. Fig. 1(a) shows the particle morphology of CeO_2 powders, it displays a nearly spherical morphology with a size in the range 50–100 nm except for a small number of aggregations. Comparing with Fig. 1(b), it can be found the Eu_2O_3 powder displays a uniform distributions and spherical morphology with a size of 40 nm, some of them are adhered together to show a liner shape.

3.2. Phase identification of RB_6 nanocrystals

Fig. 2(a) shows the XRD patterns of CeB_6 prepared at 1000–1150 °C holding for 2 h. The diffraction peaks of prepared at 1000 and 1150 °C can be assigned to the CaB_6 main phase and small amounts of $LaBO_3$ impurity phase detected, which is might be needed more acid-washing to exclude them. There is also small amounts of impurity is detected from Fig. 2(b) when the EuB_6 prepared at 1100 °C. Comparing Fig. 2(a) with (b) it can be concluded that the optimization reaction temperature of CeB_6 and EuB_6 are 1100 and 1150 °C, respectively. Their diffraction peaks are well indexed and assigned to the parallel crystal plane of (1 0 0), (1 1 0), (1 1 1), (2 1 0) and (2 1 1), which belongs to the cubic crystal system with the *Pm-3m* space group.

3.3. The morphology and microstructure of RB_6 nanocrystals

In order to better obtain the information of grain sizes and typical shapes of as-synthesized RB_6 products grown under different experimental conditions, the field emission scanning electron microscopy (FESEM) are used to observe the grain morphology. It can be seen from Fig. 3(a) that the CeB_6 prepared at 1000 °C is composed of a great deal of aggregated nanoparticle and a small number of cubic body with a size of 10–20 nm shown in the upper side of magnified SEM. When the reaction temperature is increased to 1100 °C, the nanoparticle convert into small crystalline nanocube with a size of 50–100 nm shown in Fig. 3(b). But it is also found that the CeB_6 crystals are adhered together to show a less distributions and other some amounts of large-sized non-cubic morphology crystals observed in this reaction temperature of 1100 °C. The reason is might be the aggregations raw material of CeO_2 formed the non-cubic morphology of large grains, which lead to the prepared powder less uniformed and distributions.

Fig. 4 shows the FESEM image of EuB_6 prepared at 1000–1200 °C. It is interestingly found from Fig. 4(a) that there are a large number of small cubic grains not nanoparticle, which grain size in the range of 10–20 nm at the reaction temperature of 1000 °C. Subsequently, while the reaction temperature elevated to 1100 °C, the perfect small nanocubes maintained the grain size of 30 nm and cubic morphology. However, when the reaction temperature increasing to 1100 and 1200 °C, there shows an obvious grain-growth behavior, which grain size increased to 50 and 100 nm respectively. One of the important factors for the grains growth is the high specific surface and high diffusion coefficients of nanocube have cause to mass transport through lattice and grain boundaries to grain growth. Comparing the SEM observations of EuB_6 with CeB_6, we have found the EuB_6 crystals show a more uniform distribution than CeB_6. This is due to raw materials of Eu_2O_3 is more uniform than CeB_6.

In order to further study the microstructure of RB_6 nanocrystal at different reaction temperature, the TEM as an effective characterization method to be used to observe the grain morphology and crystallinity. Herein, the EuB_6 as an example to be given the analyses in Fig. 5 with the selected area electron diffraction (SAED) pattern and the high resolution TEM (HRTEM) image. It can be seen from images that it is mainly composed by the large amounts of spherical nanoparticle and small amount of nanocube with a mean size of 10 nm, which insert magnified TEM fully confirmed the degree of crystallinity. Its corresponding SAED pattern can be indexed to (2 0 0) and (2 1 0) planes, indicating at initial temperature of 900 °C the ultrafine nanoparticles and nanocrystal are coexist. While the reaction temperature increase from 900 to 1100 °C, the nanoparticle

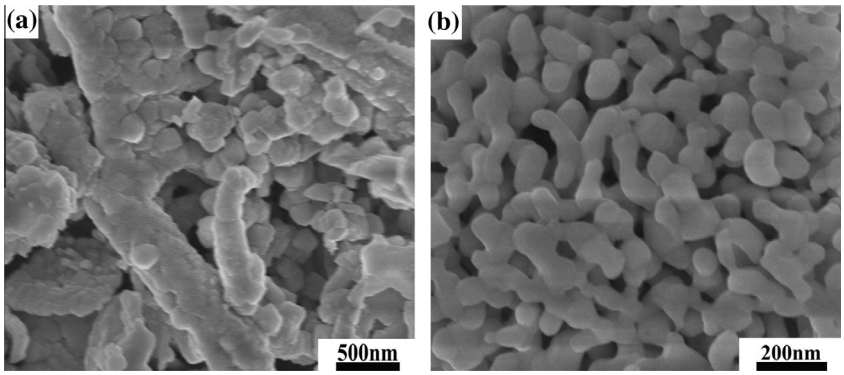

Fig. 1. FESEM image of raw materials, (a) CeO_2 and (b) Eu_2O_3.

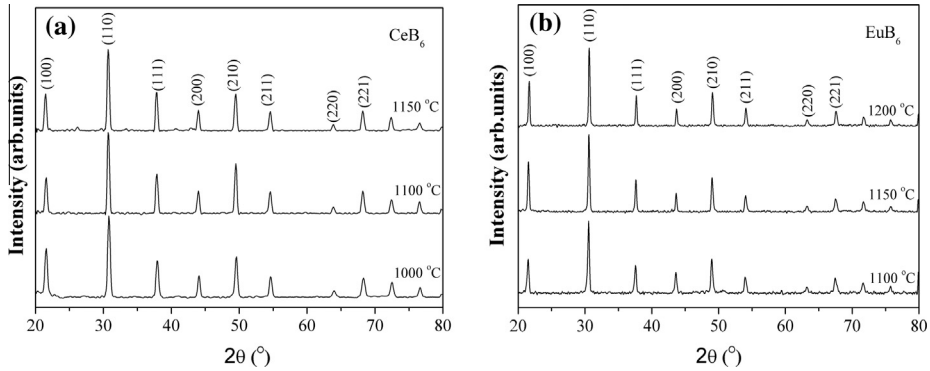

Fig. 2. XRD patterns of RB_6 nanopowders prepared at different temperature for (a) CeB_6 and (b) EuB_6 after acid-washing.

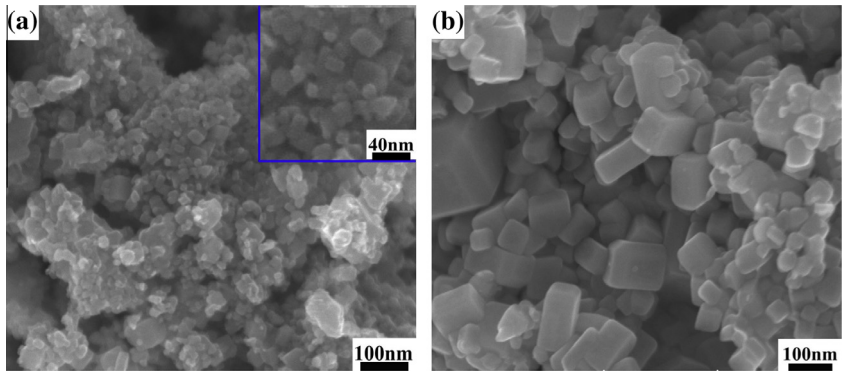

Fig. 3. FESEM images of CeB_6 prepared at (a) for 1000 °C and (b) for 1100 °C.

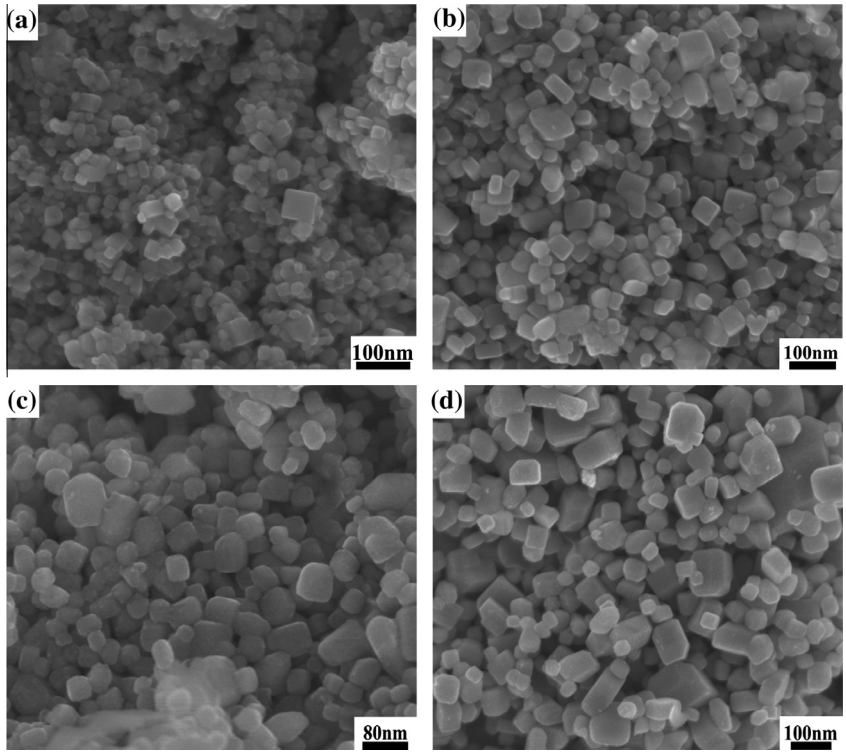

Fig. 4. FESEM images of EuB_6 prepared at (a) 1000 °C, (b) 1100 °C, (c) 1150 °C and (d) 1200 °C.

have transformed into nanocube with the mean size of 20 nm shown in Fig. 6. Its corresponding HRTEM image shows the EuB_6 nanocube displays a high crystallinity at 1100 °C, where the top right of FFT patterns reveals that the EuB_6 single crystal is mainly composed of (1 0 0) and (1 1 0) crystal planes. Fig. 7 shows the TEM images of EuB_6 prepared at 1150 °C. It can be seen that the grain size

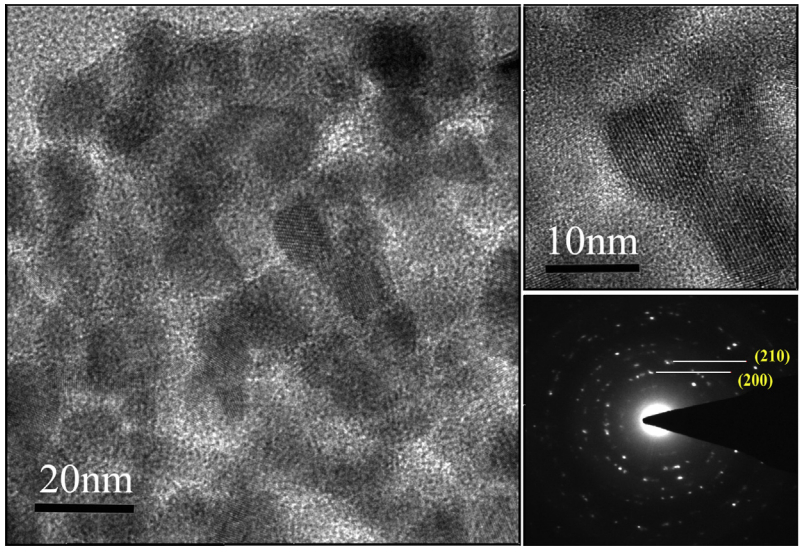

Fig. 5. TEM analyses of EuB_6 prepared at 900 °C for 2 h with the SAED pattern of the powder and its indexing (down left) and the HRTEM image (top right).

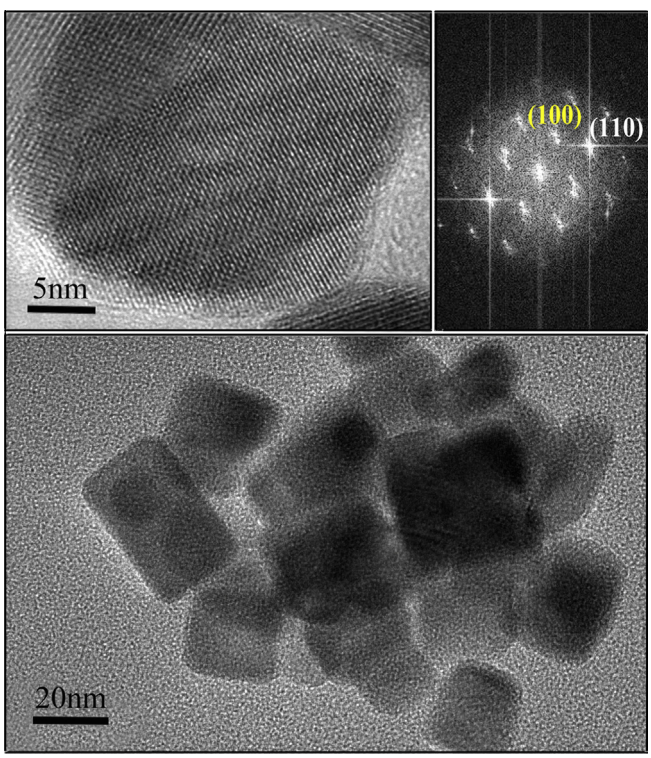

Fig. 6. TEM analyses of EuB_6 prepared at 1100 °C for 2 h with the HRTEM image of nanocube (top left) and the FFT patterns (top right).

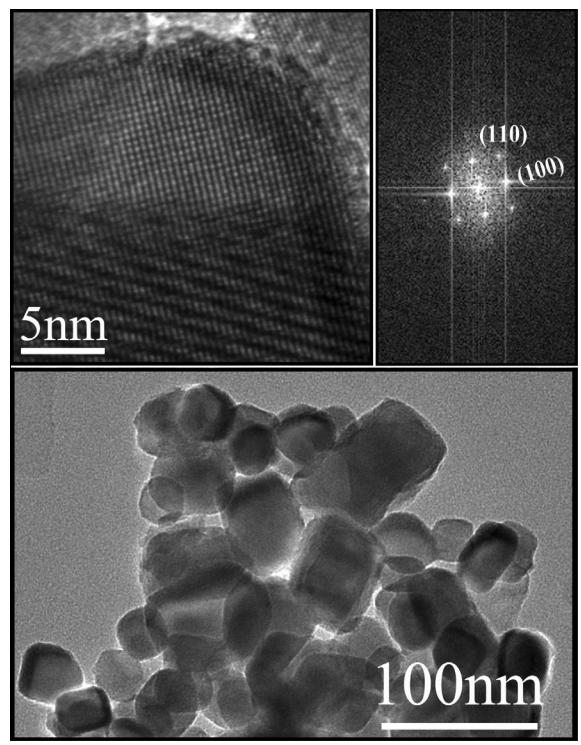

Fig. 7. TEM analyses of EuB_6 prepared at 1150 °C for 2 h with the HRTEM image of nanocube (top left) and the FFT patterns (top right).

obviously increase to 50 nm, which is agreement with SEM results, and FFT patterns confirm the cubic structure. Based on the above HRTEM analysis, it can be concluded that, the EuB_6 ultrafine nanoparticles transformed into nanocube when the reaction temperature increase from 900 to 1150 °C.

3.4. Valence state characterizations of RB_6 nanocrystals

It is well known that the valence state of rare-earth element in raw materials is a key factor for whether obtaining the RB_6 products in the reduction reaction. In order to clarify the valence state of raw materials and reaction products, the X-ray absorption near edge structure (XANES) technique was used to obtain the information on the electronic state of element such as valence and coordination environment. Fig. 8 describes the normalized XANES spectra μ(E) around the rare earth (R) L_3 edge for raw materials and reaction products, respectively, where the date of LaB_6 and NdB_6 is just for comparison with CeB_6. It can be seen from the upper layer in Fig. 8 that there is obvious one extra peak at the position of 5487 eV and 6212 eV for La_2O_3 and Nd_2O_3, respectively. Based on the investigation of Aritani et al. [31] and Choi et al. [32], these peaks representing the La and Nd located in the trivalent state, which come from the excitation from $2P_{3/2}$ to $5d$ orbitals. However, the two peaks locate in the position of 5728 eV and 5736 eV from the CeO_2 spectra, indicating a characteristic of mixed valence state.

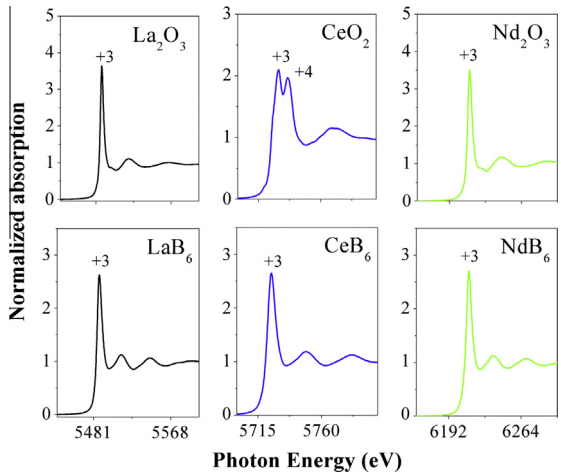

Fig. 8. Normalized XANES spectra around the R L_3 edge for raw materials and RB_6.

According to the work of Li et al. [33], the two peaks of CeO_2 are attributed by the Ce trivalent and tetravalent states, which come from the excitation from $2P_{3/2}$ to $5d$ orbitals with final state $4f^1$. Comparing with the XANES spectra in the lower layer of Fig. 8, it is found that there are single spectra peak observed at 5487, 5728 and 6212 eV for LaB_6, CeB_6 and NdB_6, respectively. It indicates the rare-earth elements are in the trivalent state in these hexaborides. Therefore, based on the above analysis, it can be confirmed that the rare-earth hexaborides such as CeB_6 not only can be synthesized by trivalent raw materials, but also by tetravalent raw materials, which opens a new preparation route for nanomaterials with a wide range of possible applications.

3.5. The reaction mechanism for RB_6 nanocrystals

In the whole synthesis procedure, it is believed that the nanocrystalline RB_6 were obtained by a solid-state reactions of rare-earth oxide with $NaBH_4$, where must be a strong reducing agent. Thus, the proposed reaction mechanism for forming RB_6 is concluded as follows:

$$NaBH_4(S) = Na(S) + B(S) + 2H_2(g) \quad (1)$$

At initial chemical reaction procedure, the $NaBH_4$ is decomposed to H_2 gas, B and Na when increasing temperature to around 900 °C as shown in Eq. (1). Due to the boiling point of Na is about 882.9 °C, so it evaporated at 900 °C and then deposited at the lower temperature side, which is observed after the reaction.

$$2R_2O_3(S) + 3H_2(g) + 18B(S) = 3RB_6(S) + 3H_2O(g) + RBO_3(S) \quad (2)$$

At second step, the rare-earth oxides are reduced by the strong reducing agent of H_2, and then the H_2 gas reacts with O to form H_2O at an elevated reaction temperature as described in Eq. (2). The gaseous H_2O is removed by vacuum pump and the impurity RBO_3 phase is removed by hydrochloric acid washing. While the mixed valences of CeO_2 as raw materials, there is an additional reducing reactions as follows:

$$Ce^{4+} + H_2 + B \rightarrow CeB_6 + H^+ \quad (3)$$

4. Conclusions

In summary, a new preparation method for RB_6 nanocrytals has been successfully developed. The method shows the advantages of single step, low cost and grain size controlled. The nanocrystalline RB_6 has perfect cubic grain morphology and the reaction temperature has a significant effect on the grain size and morphology. For EuB_6 crystal, while the reaction temperature increasing from 900 to 1150 °C, the ultrafine-nanoparticles transformed into nanocube. XANES spectra show that the rare-earth elements are in the state of trivalent state in the hexaborides and the CeB_6 also can be prepared by tetravalent raw materials. Thus, in present work, this new preparation route is significantly important for the developing new rare-earth nanomaterials with a wide range of possible applications.

Acknowledgements

This work is supported by Fundamental Research Open Project of Inner Mongolia (Grant No. 20130902), National Natural Science Foundation of China (Nos. 51161017 and 51302129).

References

[1] J.Q. Xu, Y.M. Zhao, Q.Y. Zhang, J. Appl. Phys. 104 (2008) 124306.
[2] X.J. Wang, Y.D. Jiang, Z.L. Lin, K.C. Qi, B.L. Wang, J. Phys. D: Appl. Phys. 42 (2009) 055409.
[3] K. Togawa, T. Shintake, T. Inagaki, K. Onoe, T. Tanaka, Phys. Rev. ST Accel. Beams 10 (2007) 020703.
[4] J.M. Lafferty, J. Appl. Phys. 22 (1951) 299.
[5] M. Dzero, K. Sun, P. Coleman, V. Galitski, Phys. Rev. B 85 (2012) 045130.
[6] T. Caldwell, A.P. Reyes, W.G. Moulton, P.L. Kuhns, M.J.R. Hoch, P. Schlottmann, Z. Fisk, Phys. Rev. B 75 (2007) 075106.
[7] E. Frantzeskakis, N. de Jong, B. Zwartsenberg, Y.K. Huang, Y. Pan, X. Zhang, J.X. Zhang, F.X. Zhang, L.H. Bao, O. Tegus, A. Varykhalov, A. de Visser, M.S. Golden, Phys. Rev. X 3 (2013) 041024.
[8] A. Barla, J. Derr, J.P. Sanchez, B. Salce, G. Lapertot, B.P. Doyle, R. Rüffer, R. Lengsdorf, M.M. Abd-Elmeguid, J. Flouquet, Phys. Rev. Lett. 94 (2005) 166401.
[9] Jolanta Stankiewicz, Marco Evangelisti, Zachary Fisk, Phys. Rev. B 83 (2011) 113108.
[10] J.S. Rhyee, C.A. Kim, B.K. Cho, H.C. Ri, Phys. Rev. B 83 (2002) 113108.
[11] H. Zhang, Q. Zhang, G.P. Zhao, J. Tang, O. Zhou, L.C. Qin, J. Am. Chem. Soc. 127 (2005) 13120.
[12] E.K. Storms, B.A. Mueller, J. Appl. Phys. 52 (1981) 2966.
[13] H. Zhang, Q. Zhang, J. Tang, L. Chang Qin, J. Am. Chem. Soc. 127 (2005) 2862.
[14] H. Zhang, Q. Zhang, G.P. Zhao, J. Tang, O. Zhou, L.C. Qin, Adv. Mater. 18 (2006) 87.
[15] J.Q. Xu, G.H. Hou, T. Mori, H.Q. Li, Y.R. Wang, Y.Y. Chang, Y.S. Luo, B.H. Yu, Y. Ma, T.Y. Zhai, Adv. Funct. Mater. 23 (2013) 5038.
[16] J.R. Brewer, R.M. Jacobberger, D.R. Diercks, C.L. Cheung, Chem. Mater. 23 (2011) 2606.
[17] Ramakrishnan Kalai Selvan, Isaschar Genish, Ilana Perelshtein, Jose M. Calderon Moreno, Aharon Gedanken, J. Phys. Chem. C 112 (2008) 1795.
[18] Y.F. Yuan, L. Zhang, L.M. Liang, K. He, R. Liu, G.H. Min, Ceram. Int. 37 (2011) 2891.
[19] M.F. Zhang, Y. Jia, G.G. Xu, P.F. Wang, X.Q. Wang, S.L. Xiong, X.J. Wang, Y. T Qian, Eur. J. Inorg. Chem. (2010) 1289.
[20] M.F. Zhang, L. Yuan, X.Q. Wang, H. Fan, X. Y Wang, X.Y. Wu, H.Z. Wang, Y.T. Qian, J. Solid State Chem. 181 (2008) 294.
[21] S. Kimura, T. Nanba, S. Kunii, T. Suzuki, T. Kasuya, Solid State Commun. 75 (1990) 717.
[22] H. Takeda, H. Kuno, K. Adachiw, J. Am. Ceram. Soc. 91 (2008) 2897.
[23] Y.F. Yuan, L. Zhang, L.J. Hu, W. Wang, G.H. Min, J. Solid State Chem. 184 (2011) 3364.
[24] B.H. Lai, D.H. Chen, Acta Biomaterialia. 9 (2013) 7556.
[25] T.T. Shen, D.H. Xiao, X.Q. Ou, M. Song, Y.H. He, N. Lin, D.F. Zhang, J. Alloys Comp. 509 (2011) 1236.
[26] M. Hasan, H. Sugo, E. Kisi, J. Alloys Comp. 578 (2013) 176.
[27] A. Aprea, A. Maspero, N. Masciocchi, A. Guagliardi, A.F. Albisetti, G. Giunchi, Solid State Sci. 21 (2013) 32.
[28] S.Q. Zheng, G.H. Min, Z.D. Zou, H.S. Yu, J.D. Han, J. Am. Ceram. Soc. 84 (2001) 2725.
[29] M. Aksu, E. Aydln, J. Ceram. Process. Res. 14 (2013) 4.
[30] H. Zhang, Q. Zhang, J. Tang, L.C. Qin, J. Am. Chem. Soc. 127 (2005) 8002.
[31] H. Aritani, H. Yamada, T. Yamamoto, T. Tanaka, S. Imamura, J. Synchrotron Rad. 8 (2001) 593.
[32] Y.G. Choi, K.A. Lee, K.S. Lee, Met. Mater. Int. 4 (2007) 269.
[33] Y.J. Li, O. Naoyuki, N. Ikuo, N. Yusuke, M. Shigeyuki, J. Phys. Soc. Jpn. 78 (2009) 094717.